The role of a conserved tyrosine residue in high-potential iron sulfur proteins

ARTICLE *in* PROTEIN SCIENCE · DECEMBER 1995

Impact Factor: 2.85 · DOI: 10.1002/pro.5560041213 · Source: PubMed

7 AUTHORS, INCLUDING:

Isabella Felli
University of Florence
102 PUBLICATIONS **2,971** CITATIONS
SEE PROFILE

Mario Piccioli
University of Florence
99 PUBLICATIONS **2,309** CITATIONS
SEE PROFILE

Protein Science (1995), *4*:2562–2572. Cambridge University Press. Printed in the USA.

The role of a conserved tyrosine residue in high-potential iron sulfur proteins

SAKURA G. IWAGAMI,[1,5] A. LOUISE CREAGH,[1] CHARLES A. HAYNES,[1] MARCO BORSARI,[2] ISABELLA C. FELLI,[3] MARIO PICCIOLI,[3] AND LINDSAY D. ELTIS[1,4]

[1] Biotechnology Laboratory, University of British Columbia, Vancouver, British Columbia V6T 1Z3, Canada
[2] Department of Chemistry, University of Modena, Via Campi 183, 41100 Modena, Italy
[3] Department of Chemistry, University of Florence, Via Gino Capponi 7, 50121 Florence, Italy
[4] Department of Biochemistry, Université Laval, Ste-Foy, Québec G1K 7P4, Canada

(RECEIVED June 22, 1995; ACCEPTED September 29, 1995)

Abstract

Conserved tyrosine-12 of *Ectothiorhodospira halophila* high-potential iron sulphur protein (HiPIP) iso-I was substituted with phenylalanine (Y12F), histidine (Y12H), tryptophan (Y12W), isoleucine (Y12I), and alanine (Y12A). Variants Y12A and Y12I were expressed to reasonable levels in cells grown at lower temperatures, but decomposed during purification. Variants Y12F, Y12H, and Y12W were substantially destabilized with respect to the recombinant wild-type HiPIP (rcWT) as determined by differential scanning calorimetry over a pH range of 7.0–11.0. Characterization of the Y12F variant by NMR indicates that the principal structural differences between this variant and the rcWT HiPIP result from the loss of the two hydrogen bonds of the Tyr-12 hydroxyl group with Asn-14 Oδ1 and Lys-59 NH, respectively. The effect of the loss of the latter interaction is propagated through the Lys-59/Val-58 peptide bond, thereby perturbing Gly-46. The $\Delta\Delta G_D^{app}$ of Y12F of 2.3 kcal/mol with respect to rcWT HiPIP (25 °C, pH 7.0) is entirely consistent with the contribution of these two hydrogen bonds to the stability of the latter. CD measurements show that Tyr-12 influences several electronic transitions within the cluster. The midpoint reduction potentials of variants Y12F, Y12H, and Y12W were 17, 19, and 22 mV (20 mM MOPS, 0.2 M sodium chloride, pH 6.98, 25 °C), respectively, higher than that of rcWT HiPIP. The current results indicate that, although conserved Tyr-12 modulates the properties of the cluster, its principle function is to stabilize the HiPIP through hydrogen bonds involving its hydroxyl group and electrostatic interactions involving its aromatic ring.

Keywords: ferredoxin; hydrogen bonds; protein engineering; thermodynamic stability; site-directed mutagenesis

High-potential iron sulphur proteins (HiPIPs) are a class of small electron transfer metalloproteins that have been predominantly found in purple sulfur bacteria (Bartsch, 1978). The cubane [4Fe-4S] cluster of HiPIPs is widespread in nature, functioning in electron transfer, catalytic, or other roles in various proteins including ferredoxins, hydrogenase (Volbeda et al., 1995), aconitase (Beinert & Kennedy, 1989), and gene regulatory proteins (Khoroshilova et al., 1995). In addition, the [4Fe-4S] cluster is an element of more complex centers such as the P-cluster of nitrogenase (Kim & Rees, 1992). HiPIPs are amenable to study by a variety of biophysical techniques, and are thus important paradigms in elucidating the structural determinants of the physicochemical properties of both [4Fe-4S] clusters and, more generally, biological metallocenters.

As their name implies, HiPIPs have relatively high midpoint reduction potentials, varying between 50 and 450 mV (Przysiecki et al., 1985). The cluster of the reduced HiPIP has an overall charge of +2 and a net spin of 0 (Carter et al., 1972; Antanaitis & Moss, 1975). Mössbauer spectra indicate that the iron atoms are in equivalent, $Fe^{2.5+}$, oxidation states (Middleton et al., 1980). The oxidized HiPIP cluster, with an overall charge of +3 and a net spin of 1/2, is made up of two antiferromagnetically coupled spin pairs. One spin pair consists of two Fe^{3+}, whereas the other consists of two $Fe^{2.5+}$ (Middleton et al., 1980). The chemical shift of the βCH_2 protons of the cluster cysteine ligands and their temperature dependence are consistent with this interpretation (Bertini et al., 1991). Extensive NMR work demonstrates that the position of the spin pairs within the protein framework varies from one HiPIP to another

Reprint requests to: Lindsay D. Eltis, Department of Biochemistry, Université Laval, Ste-Foy, Québec G1K 7P4, Canada; e-mail: leltis@rsvs.ulaval.ca.

[5] Present address: Department of Microbiology and Immunology, University of British Columbia, Vancouver, British Columbia V6T 1Z3, Canada.

(Bertini et al., 1995a), and may be determined by the relative reduction potentials of the individual iron atoms (Babini et al., in press). A third oxidation state of the [4Fe-4S] cluster possesses a charge of +1. This corresponds to the reduced ferredoxin cluster and has only been observed in HiPIPs when the protein is partially denatured (Cammack, 1973).

From the crystallographic and solution structures of four HiPIPs (Carter et al., 1974b; Breiter et al., 1991; Rayment et al., 1992; Benning et al., 1994; Banci et al., 1994, 1995a), it is clear that HiPIPs share many tertiary structural elements, including a cluster that is sequestered from the solvent and a network of hydrogen bonds between the backbone amides and the cluster sulfur atoms (Kinemage 1). These structural features, confirmed by resonance Raman (Backes et al., 1991) and electron spin echo studies (Orme-Johnson et al., 1983), were first proposed as determinants of the accessible oxidation states of [4Fe-4S] cluster in HiPIPs versus ferredoxins more than 20 years ago (Carter et al., 1972). This view has recently been refined by protein-dipole Langevin dipole calculations, a study in which the role of the polarity of the amide groups surrounding the cluster in determining the reduction potential of the latter was stressed (Jensen et al., 1994). Although HiPIPs share considerable similarity in their tertiary structures, they show surprising variability in their amino acid sequences and overall charges. This variability in overall charges has been cited as a determinant in the range of their reduction potentials (Banci et al., 1995b).

Despite the extensive characterization of HiPIPs, there exists little direct experimental evidence identifying the structural determinants of the properties of the cluster. Synthetic genes encoding two HiPIPs have been expressed (Agarwal et al., 1993; Eltis et al., 1994) and are being used to provide such evidence (Lui & Cowan, 1994; Babini et al., in prep.). In this context, we investigated the role of tyrosine-12 in *Ectothiorhodospira halophila* HiPIP-I (Fig. 1). This residue corresponds to Tyr-19 of *Chromatium vinosum* HiPIP and is the only conserved residue in HiPIPs other than the four cysteines that ligate the cluster, although Gly-62 is conserved in all HiPIPs sequenced to date except the large and small HiPIPs of *E. salinarum* (R.P. Ambler, pers. comm.). Tyr-12 is proposed to contribute to the spectroscopic and electrochemical properties of the cluster (Carter, 1977; Przysiecki et al., 1985; Lui & Cowan, 1994). In the present study, the role of Tyr-12 of *E. halophila* HiPIP-I was investigated by replacing this residue with phenylalanine, histidine, tryptophan, isoleucine, and alanine by oligonucleotide-directed mutagenesis. The variants were purified and the effects of the substitutions on the CD spectra, the midpoint reduction potential, the thermostability, and the structure of the protein were investigated.

Table 1. *Sequences of oligonucleotides used to introduce substitutions at position 12 of E. halophila HiPIP-I*[a]

Variant	Plasmid	Oligonucleotide
Y12F	pSIHP1	5′-TTCGTTAACG**AA**GTCGTGAGC-3′
Y12W	pSIHP7	5′-CTTCGTTAAC**CC**AGTCGTGAGC-3′
Y12H	pSIHP4	5′-TCGTTAACGTGGTCGTGAGCG-3′
Y12A	pSIHP2	5′-TTCGTTAACGGC**G**TCGTGAGCG-3′
Y12I	pSIHP3	5′-TTCGTTAACG**AT**GTCGTGAGCG-3′

[a] Nucleotides differing from the sequence of the gene encoding rcWT are shown in boldface.

Results

Expression and purification of position-12 variants

Expression of Y12F, Y12H, and Y12W variant HiPIPs was detected in small-scale cultures of XL-1 Blue cells containing pSIHP1, pSIHP4, and pSIHP7, respectively (see Table 1). No recombinant protein was detected in XL-1 Blue cells containing pSIHP2 or pSIHP3, although expression was tested at various times after induction with IPTG. The genes encoding Y12A and Y12I were recloned into pLEHP20 to verify that the lack of detection of these variants in cellular extracts was not due to mutations in parts of the plasmid for which sequence information was not obtained. The genes encoding Y12A and Y12I were cloned into pT7-7 on an *Xba* I–*Hin*d III fragment, yielding pSIHP5 and pSIHP6, respectively. The expression of variant HiPIPs was detected in BL21(DE3) cells containing pSIHP5 or pSIHP6. As exemplified in Figure 2, at 37 °C, the expression of Y12A or Y12I variants was detected up to 3 h after the addition of IPTG to the culture, but not after 24 h. Incubation of the in-

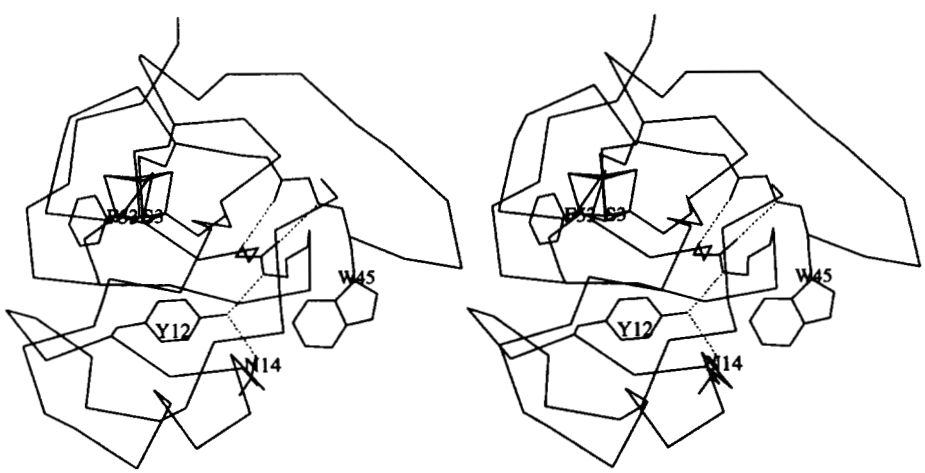

Fig. 1. Structure of oxidized recombinant *E. halophila* HiPIP iso-I around Tyr-12. The structure depicts the backbone trace and cluster atoms, and the side chains of the Cys ligands, Tyr-12, Asn-14, and Trp-45. Four hydrogen bonds are shown as dotted lines: the two involving the hydroxyl group of Tyr-12 and the two between the backbone atoms of Val-58 and Gly-46. Coordinates were taken from Bertini et al. (1995b).

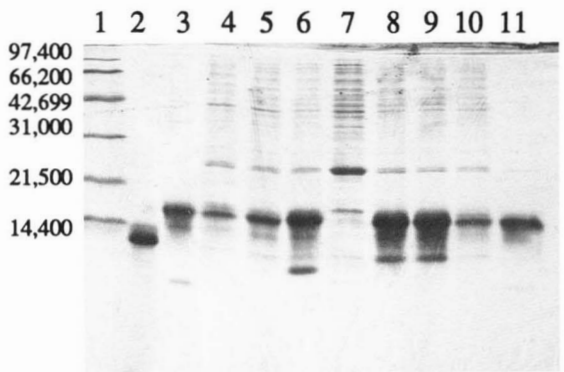

Fig. 2. Expression of Y12A and Y12H variants of *E. halophila* HiPIP iso-I 17% SDS-PAGE of nickel resin extracts from appropriately induced cells. Lane 1 was loaded with Bio-Rad low molecular weight markers, lane 2 was loaded with purified, cleaved Y12F, and lane 3 was loaded with uncleaved rcWT HiPIP. Lanes 4–7 were loaded with extracts of BL21(DE3) harboring pSIHP5 incubated at 37 °C, 0.5, 1, 3, and 24 h after induction with 1 mM IPTG. Lanes 8–10 were loaded with extracts of BL21(DE3) harboring pSIHP5 incubated at 25 °C, 3, 6, and 24 h after induction with 1 mM IPTG. Lane 11 contains an extract from XL-1 Blue incubated at 37 °C for 24 h after induction with 1 mM IPTG.

duced cultures at 25 °C resulted in significantly higher levels of expression of these variants for at least 6 h after induction, and recombinant protein persisted for at least 24 h after the addition of IPTG to the culture.

The Y12F variant was purified from cells harvested from a 10-L culture of pSIHP1/XL-1 Blue cells induced with IPTG at an OD_{600} of approximately 2. This culture yielded 32 g of cells (wet weight) from which 86 mg of Y12F variant was purified to apparent homogeneity. The UV-visible absorption spectrum of this protein was virtually identical to that of the rcWT, and, in the oxidized state, had an *R*-value of 2.1 (20 mM MOPS, pH 7.0, 25 °C).

Y12H bound to the nickel resin as a greenish-brown band that was lighter in color than comparable preparations of Y12F or rcWT. The HiPIP was eluted from this column as a yellow protein fraction with an *R*-value of 3.2. During subsequent concentration and dialysis at 4 °C, the *R*-value of this protein rose to 17.2. Due to the apparent instability of Y12H, this variant was purified with argon-purged buffers as described in the Materials and methods. Twelve milligrams of Y12H, possessing an *R*-value of 2.45 (20 mM MOPS, pH 7.0), was obtained from 2 L of cell culture.

Similarly, the Y12W variant was found to be unstable during aerobic purification. Using the semi-anaerobic purification protocol, 196 mg of apparently homogeneous protein was obtained from a 20-L culture (*R*-value of 2.66 in 20 mM MOPS, pH 7.0).

BL21(DE3) cells expressing Y12A and Y12I HiPIP variants were grown in 5-L cultures at 37 °C to an OD_{600} of 1 and induced with IPTG. Cultures were then incubated for an additional 6 h at 25 °C and harvested. Approximately 20 g of wet cell paste was obtained from each culture. The recombinant HiPIP variants were observed to bind as a greenish-brown band to the top of a column of Pro-Bond resin. After dialysis of the HiPIPs into cleavage buffer, the solution containing the Y12A variant was yellow-green in color, whereas that containing Y12I was a light green-brown in color. The color of the preparation of rcWT and Y12F HiPIP at this stage is dark brown. During the subsequent concentration of the variant HiPIPs, the *R*-value of the Y12I preparation rose from 5.9 to 25.5, and a red-brown precipitate formed in the concentration vessel. Similarly, during the concentration of Y12A, the *R*-value of the protein rose from 6.9 to 9.1, and a green-brown precipitate formed. In contrast, the *R*-value of Y12F was approximately 2.3 after elution from the nickel resin and remained unchanged during dialysis and concentration. These observations indicate that the Y12A and Y12I variants lost their chromophore during purification and that the proteins are not stable under these conditions. Further characterization of these variant HiPIPs was not undertaken.

^{1}H-NMR spectroscopy

Due to the lability of Y12F, it was not possible to collect the data necessary to solve the three-dimensional structure of the variant at a resolution comparable to that of the rcWT (Banci et al., 1994). Nevertheless, the comparison of 2D NOESY maps collected on the reduced form of rcWT and Y12F permitted the assignment of most of the proton resonances of the Y12F variant: of 350 resonances assigned in rcWT, 315 were assigned in Y12F (approximately 90%). Of these 315 commonly assigned resonances, 75% have chemical shifts that differ by less than 0.04 ppm between the two proteins. The HN resonance and one of the Hβ protons of Phe-12 in Y12F have the same chemical shifts as the corresponding Tyr-12 resonances in rcWT. Most of the cross peaks observed in the NOESY spectra of reduced rcWT are quantitatively and qualitatively retained in Y12F. This indicates that the overall fold of the HiPIP is conserved in the variant. Apart from the signals of cysteine residues, proton chemical shifts that differ by more that 0.15 ppm in the spectrum of reduced Y12F as compared to the same signals in the spectrum of rcWT are listed in Table 2. Eleven protons (i.e., 3.5% of the assigned resonances) fall into this category and are assumed to reside in the regions most affected by the substitution. Two of these protons are on Gly-46 and Val-58. Interestingly, some of the NOESY connectivities involving Gly-46 differ from rcWT to Y12F. The same is observed for some connectivities involving Ala-60 Hα.

Table 2. *Chemical shift differences in Y12F versus rcWT*[a]

Proton	δ in rcWT (ppm)	δ in Y12F (ppm)	Difference (ppm)
Ala-4 HN	9.54	9.75	−0.21
Glu-5 HN	8.92	9.19	−0.27
Asn-14 HD22	7.46	7.17	0.29
Asn-14 HA	4.38	4.12	0.26
Glu-39 HN	6.18	6.02	0.16
Trp-45 HA	5.49	5.32	0.17
Trp-45 HE1	10.33	10.50	−0.17
Gly-46 HN	10.38	9.98	0.40
Arg-49 HA	4.20	4.42	−0.22
Val-58 HN	8.90	9.14	−0.24
Lys-59 HA	3.79	3.60	0.19

[a] Based on measurements performed on reduced HiPIPs. Only those chemical shifts that differ by more than 0.15 ppm are reported. Errors in the chemical shifts were less than 0.005 ppm.

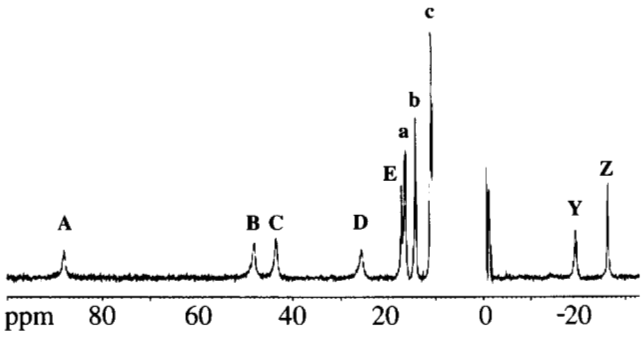

Fig. 3. ^{1}H NMR, 600 MHz spectrum of a 65% reduced, 35% oxidized sample of Y12F variant of *E. halophila* HiPIP iso-I at pH 5.0 and 15 °C. Signals labeled with lower-case letters arise from the reduced form of the protein and their assignment is reported in Table 3. Signals labeled with upper-case letters arise from the oxidized form of the protein and their assignment is reported in Table 4.

The cluster-coordinated cysteine resonances are sensitive monitors of the ligand geometry and electron distribution within the cluster. Figure 3 shows the ^{1}H NMR spectra of a sample of partially oxidized Y12F, permitting the observation of hyperfine shifted signals arising from both oxidation states. These signals are easily assigned by comparison to the spectra of rcWT. Table 3 summarizes the chemical shifts of the βCH_2 protons of reduced Y12F and the differences of these chemical shifts with respect to rcWT (pH 5.0, 15 °C). In reduced HiPIPs, the chemical shifts of cysteine βCH_2 protons are related to the Fe-S-C-H dihedral angle by a Karplus-type relationship (Bertini et al., 1994a). For the three observable Cys residues, the variation in the calculated Fe-S-C-H dihedral angles in Y12F and rcWT differ by less than 3°, and therefore are not significant.

The chemical shifts of the Cys βCH_2 protons in the oxidized HiPIPs and the behavior of these signals as a function of temperature are sensitive probes of the electronic configuration of the cluster. Inspection of the oxidized Y12F variant spectrum shows that the βCH_2 protons of Cys-34 are essentially unaffected (less than 3% of the relative hyperfine shift) by the replacement of Tyr-12 with phenylalanine (Table 4). The protons of the other three cysteines experience changes in their respective chemical shifts that range between 2.6 and 11%. Averaging the observed percent change of the chemical shift on a per residue basis (i.e., βCH_2 of Cys-31, βCH_2 of Cys-48, and αCH of Cys-64) reveals a change of 7.3% for Cys-31, 8.5% for Cys-48, and 10% for Cys-64. The βCH_2 of Cys-64 are not included in this analysis because the chemical shift of these signals is such

Table 3. *Variation of chemical shifts of hyperfine shifted signals in reduced Y12F*[a]

Signal	Assignment	rcWT	Y12F	Difference	Change in dihedral angle
a	Cys-31 Hβ2	16.56	16.41	−0.15	−0.7
b	Cys-48 Hβ2	14.07	14.28	0.21	1.3
c	Cys-64 Hβ2	10.77	11.08	0.31	−2.9

[a] Recorded at pH 5.0, 15 °C.

Table 4. *Variation of chemical shifts of hyperfine shifted signals in oxidized Y12F*

Signal	Assigment	rcWT	Y12F	Percent difference
A	Cys-48 Hβ2	93.45	88.08	−5.9
B	Cys-34 Hβ2	46.95	48.09	2.6
C	Cys-34 Hβ1	42.44	43.48	2.7
D	Cys-48 Hβ1	28.54	25.67	−11.1
E	Cys-64 Hα	15.99	17.21	10.3
Y	Cys-31 Hβ2	−22.36	−19.45	11.6
Z	Cys-31 Hβ1	−27.17	−26.25	3.1

[a] Recorded at pH 5.0, 15 °C.

that they occur under the diamagnetic envelope of the protein (Bertini et al., 1995a). The degree to which the hyperfine chemical shifts are influenced by substitution at position 12 is consistent with location of this residue in the protein. Tyr-12 is on the opposite side of the cluster with respect to Cys-34 and approximately equidistant from the three other cysteinyl ligands (Kinemage 1). The magnitude of the effect is small and does not alter the relative order of the hyperfine shifted signals. The temperature dependence of the chemical shifts of the hyperfine shifted signals in Y12F is identical to those of rcWT (data not shown). Interestingly, the chemical shifts of the hyperfine shifted signals show a stronger pH dependence in oxidized Y12F than rcWT.

Differential scanning microcalorimetry

Figure 4 shows differential scanning microcalorimetry (DSC) thermograms for rcWT *E. halophila* HiPIP-I at pH 7 and pH 11. At pH 7 and above, the thermal denaturation of rcWT HiPIP is highly exothermic and, as discussed below, irreversible. This behavior has been observed for adrenodoxin, a [2Fe-2S] protein, in which the exothermic peak and irreversibility of thermal denaturation appears to be associated with the disruption of the prosthetic cluster (Burova et al., 1995). The exothermic

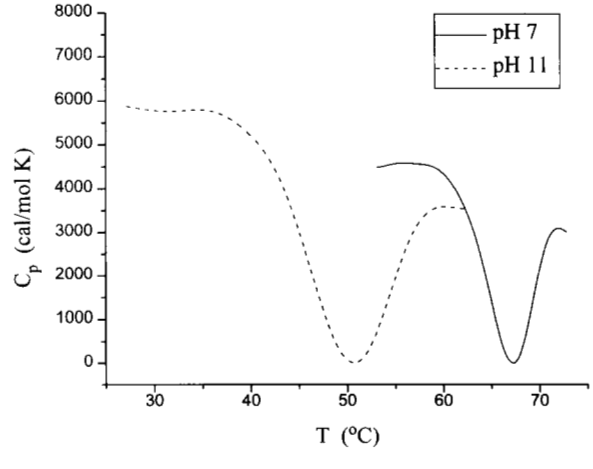

Fig. 4. DSC scans of rcWT *E. halophila* HiPIP iso-I at pH 7.0 (20 mM MOPS) and 11.0 (40 mM piperidine).

peak is superimposed on a conventional endothermic peak characterizing denaturation of the native protein superstructure.

Denaturation enthalpies and temperatures of rcWT show a very small scan-rate dependence over the range of 0.5–1.5 °C/min, indicating that the conversion to the final unfolded state is kinetically controlled (Freire et al., 1990). At all the solution pH's tested here, the thermal unfolding of rcWT is reversible up to the measured denaturation temperature for the protein. The denaturation proceeds to an irreversible unfolded state if the thermogram is allowed to proceed beyond the temperature at which the peak maximum occurs. This behavior is consistent with the model proposed by Freire and Biltonen (1978), which assumes that such a denaturation is a multi-step process in which the protein proceeds reversibly through one or more unfolded intermediates before undergoing an irreversible transition to a final unfolded state. For our system, a three-step model was assumed with step 1 being the reversible, endothermic denaturation of the polypeptide; step 2, the exothermic release of the [4Fe-4S] cluster; and step 3, an irreversible transition to the final state at high temperatures. Consistent with a similar study by Freire et al. (1990), application of this model to our data yielded thermodynamic results (e.g., $\Delta\Delta G_D$) that were identical with those calculated assuming the irreversible process has no thermal effect. Thus, a two-stage form of the reversible thermodynamic model of Freire and Biltonen (1978) provides a reasonable description of the unfolding process. Regression of the thermal scan data assuming a first-order kinetic process with a temperature dependence to the rate constant k given by the Arrhenius equation yields a frequency factor, ln A, of 28.4 and an activation energy of approximately 16 kcal/mol.

Table 5 shows average denaturation temperatures (T_m) for rcWT and position-12 variant HiPIPs as a function of solution pH. At equivalent pH, the denaturation temperature of each variant is substantially lower than the corresponding T_m for rcWT, with the Y12W giving the most dramatic changes. A small decrease or increase in T_m ($\leq$5 °C) is usually, but not always, indicative of a concomitant decrease or increase, respectively, in the Gibbs energy difference, $\Delta\Delta G_D$, stabilizing the native state of the variant relative to that of wild type. Betz and Pielak (1992), for instance, report data for variants of cytochrome *c* where the T_m of a variant increases slightly despite an observed decrease in variant stability (i.e., a positive $\Delta\Delta G_D$ value). However, large decreases in T_m (i.e., $\geq$10 °C), such as those reported here, appear to always be associated with a decrease in stability (Privalov & Potekhin, 1986; Becktel & Schellman, 1987).

Table 5. *Differential scanning calorimetric data for the unfolding of position-12 E. halophila HiPIP-I variants*[a]

	pH	T_m (°C)	$\Delta H_D^{app}(T_m)$ (kcal/mol)
rcWT	7	67.7 (0.8)	−21.7 (1.8)
	9	66.4 (0.5)	−23.0 (1.6)
	10	66.5 (0.6)	−22.9 (2.0)
	10.8	56.7 (0.4)	−33.4 (1.7)
	11	50.3 (0.6)	−40.3 (1.5)
Y12F	7	54.8 (0.5)	−21.2 (0.7)
	9	54.4 (0.6)	−20.7 (2.3)
	10	54.2 (0.4)	−24.2 (1.5)
	10.8	37.1 (0.4)	−29.2 (1.7)
Y12W	7	37.4 (0.5)	−23.7 (0.7)
Y12H	7	42.2 (0.5)	−33.3 (1.8)
	9	39.0 (0.6)	−53.3 (2.3)

[a] The uncertainties in T_m and ΔH_D^{app} are provided in parentheses.

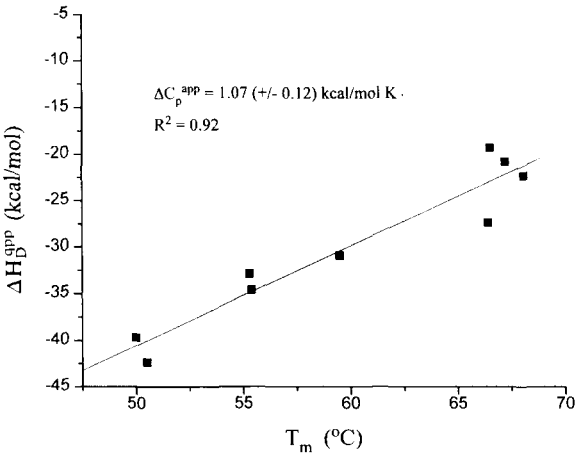

Fig. 5. Calorimetric enthalpies (ΔH_D^{app}) of rcWT *E. halophila* HiPIP iso-I as a function of melting temperature (T_m).

Although the exothermic signal associated with disruption of the [4Fe-4S] cluster prevents absolute determination of Gibbs energies of denaturation (ΔG_D) for rcWT and variant HiPIPs, "apparent" destabilization energies ($\Delta\Delta G_D^{app}$) can be established by assuming that the magnitude of the exothermic transition does not vary with pH or between HiPIP variants and applying the theory of Freire and Biltonen (1978). The thermodynamic observables in each DSC thermogram are the temperature at the midpoint of the unfolding transition T_m, and the apparent total calorimetric enthalpy of denaturation ΔH_D^{app}. Because the irreversible step in the denaturation process shows little thermal effect, regression of ΔH_D^{app} versus T_m data, as shown in Figure 5 for rcWT HiPIP, yields a straight line with slope equal to ΔC_p^{app}, the apparent heat capacity change for the unfolding reaction. Combination of these data with the thermodynamic framework described above then provides $\Delta\Delta G_D^{app}$ for each variant. The "app" superscript has been adopted here to acknowledge the fact that the Freire and Biltonen model has not been extensively tested, although the resulting thermodynamic data are consistent with other experimental observations (see Discussion).

Table 5 gives T_m and ΔH_D^{app} data for rcWT and variant HiPIPs. The regressed ΔC_p^{app} value was 1.1 (± 0.1) kcal/mol K for both rcWT HiPIP and the Y12F variant. It was assumed that ΔC_p^{app} is relatively insensitive to the substitution at position 12, and this value was used in analyzing the data of Y12H and Y12W. For each variant, Table 6 reports $\Delta\Delta G_D^{app}$ values along with the experimental error $\delta\Delta G$ calculated according to the equation

$$\delta\Delta G(T) = [1 - (T/T_m)]\,\delta\Delta H(T_m) + [(T - T_m) - T\ln(T/T_m)]\,\delta\Delta C_p \quad (1)$$

Table 6. *Changes in transition temperatures and Gibbs energy for position-12 E. halophila HiPIP-I variants*

pH	ΔT_m (°C)	$\Delta\Delta G_D^{app}$ (25 °C) (kcal/mol)	$\delta\Delta G$ (25 °C) (kcal/mol)
Y12F	7	−12.9	2.30.06
	9	−12.0	2.30.06
	10	−12.3	2.10.06
	10.8	−19.6	3.50.07
Y12W	7	−30.3	4.50.07
Y12H	7	−25.5	3.40.08
	9	−27.4	2.90.08

derived by Matouschek et al. (1994). The standard errors $\delta\Delta H(T_m)$ (error in ΔH_D) and $\delta\Delta C_p$ (error in ΔC_p^{app}) were determined from the data regression in Figure 2 to be 2.56 kcal/mol and 0.12 kcal/mol K, respectively.

CD spectroscopy of position-12 variants

The UV-visible absorption spectra of the oxidized and reduced Y12F, Y12H, and Y12W variants were essentially identical to those of the rcWT HiPIP, other than slight differences in the relative intensity of the absorption in the visible region (results not shown). The CD spectra of the variant proteins were recorded because this technique is better able to resolve the S → Fe charge transitions that give rise to the visible absorption spectrum of the [4Fe-S] cluster. The greatest differences in the CD spectra of the reduced HiPIPs are observed for Y12H and Y12W (Fig. 6A). As compared to Y12F and rcWT, the spectra of these variants show a loss of the negative bands at 310 nm, 340 nm, and 465 nm. Interestingly, the spectrum of reduced Y12W is not that much less intense than those of Y12F and rcWT between 360 and 440 nm, but the positive bands at 370 nm and 420 nm are less well resolved and slightly blue shifted. The changes in the reduced spectrum of Y12H are even greater, with a new positive band appearing at 440 nm in addition to the loss in intensity of the features at 370 nm and 405 nm. The CD spectra for the oxidized forms of rcWT and the position-12 variants were more similar (Fig. 6B), the principle difference being the decreased intensity of the positive Cotton effect of the Y12H and Y12W variants between 340 and 510 nm. The CD spectra reported here showed no variation over the course of 4 h.

Electrochemistry of Y12F, Y12H, and Y12W variant HiPIPs

Figure 7 depicts a typical cyclic voltammogram obtained in determining the midpoint reduction potentials of the rcWT and variant HiPIPs. The reduction potential of the protein and the reversibility of the electron transfer between the electrode and the protein were independent of the concentration of neomycin over a range of concentration of 0.5–4.0 mM. Beyond these concentration limits, the shape of the voltammetric signal was distorted and the reversibility was diminished. The midpoint reduction potential of rcWT HiPIP is 133 mV (25 °C, 20 mM MOPS, 200 mM sodium chloride, pH 6.98, S.H.E.). This is

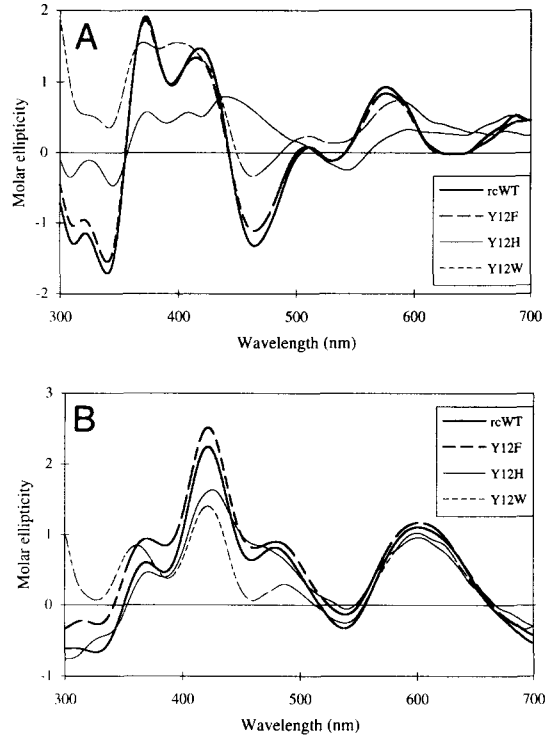

Fig. 6. CD spectra of (**A**) reduced and (**B**) oxidized rcWT and variant *E. halophila* HiPIP-I (80 mM HEPES, 0.1 M NaCl, pH 7.0, 25 °C).

somewhat higher than the value determined spectroelectrochemically (120 mV, Eltis et al., 1994), however, the solution conditions were different (20 mM MOPS, 80 mM sodium chloride, pH 7.0). Cyclic voltammetric measurements performed under these conditions have yielded the same reduction potential within ±2 mV.

As summarized in Table 7, the position-12 variants all had midpoint reduction potentials between 17 and 22 mV higher than that of rcWT. These observations agree with the spectroelectrochemically determined reduction potential of Y12F, which was 14 mV higher than that of rcWT. Inspection of the thermo-

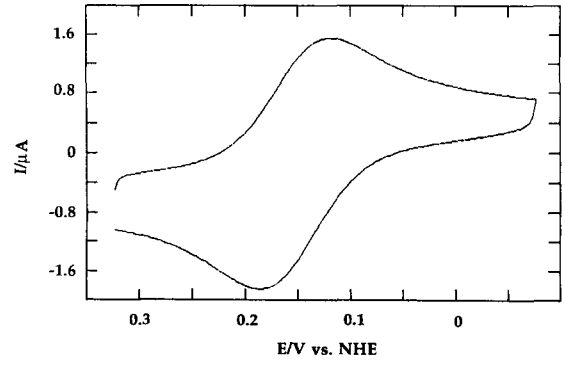

Fig. 7. Cyclic voltammogram of the Y12F variant of *E. halophila* HiPIP iso-I. The solution contained 0.2 mM protein, 20 mM MOPS, 0.2 M NaCl, pH 6.98, 25 °C. The scan rate was 0.01 V/s.

Table 7. *Electrochemical properties of position-12 E. halophila HiPIP-I variants*[a]

Variant	E° (mV vs. SHE)	$\Delta S°$ (cal mol^{-1} K^{-1})	$\Delta H°$ (kcal mol^{-1})
rcWT	133	−30.9	−12.2
Y12F	150	−28.1	−12.0
Y12W	152	−28.0	−12.0
Y12H	155	−28.2	−12.0

[a] 25 °C, 20 mM MOPS, 0.2 M NaCl, pH 6.98. The uncertainties in E°, $\Delta S°$, and $\Delta H°$ are 2 mV, 0.5 cal mol^{-1} K^{-1}, and 0.2 kcal mol^{-1}, respectively.

dynamic parameters derived from the temperature dependence of these reduction potentials reveals that the replacements at position 12 influences the reduction potential of the variants through entropic effects.

Discussion

Tyrosine-12 of *E. halophila* HiPIP iso-I (Tyr-19 in *C. vinosum* HiPIP) is the only conserved residue in HiPIPs other than the four cysteine residues that ligate the iron atoms of the cluster. Tyr-12 is one of several aromatic residues that surround the [4Fe-4S] cluster, shielding the latter from the solvent and contributing to its hydrophobic environment. Studies on *C. vinosum* HiPIP indicate that this residue, numbered 19 in the *C. vinosum* protein, is coupled to the cluster by two mutually reinforcing effects: a π–π interaction between the aromatic ring and the cluster; and polarization of the ring by the cluster, which strengthens a hydrogen bond between Oη and the NH of residue 72 (Sheridan et al., 1981). Characterization of 3-fluorotyrosine-substituted *C. vinosum* HiPIP demonstrates that Tyr-19 is electronically coupled to the cluster and that the aromatic ring has increased rotational freedom in the oxidized HiPIP (Lui & Cowan, 1994). In contrast, the ring-flipping rate of Y12 in *E. halophila* HiPIP-I is between 10 and 1,200 s^{-1} and does not appear to depend on the oxidation state of the HiPIP (Bertini et al., 1995b).

The solution structures of rcWT *E. halophila* HiPIP-I (Banci et al., 1994; Bertini et al., 1995b) and the crystal structures of *E. halophila* HiPIP-I (Breiter et al., 1991) show that Tyr-12 occupies a position that is spatially equivalent to Tyr-19 in *C. vinosum* HiPIP, with Cδ and Cϵ atoms of the Tyr-12 ring located 4.0–4.5 Å from S*3 of the cluster (Fig. 1 and Kinemage 1). The slightly positively charged ring protons can thus interact with the negatively charged S*3 sulfur. The solution structures of both the oxidized and reduced rcWT HiPIP indicate that the hydroxyl group of Tyr-12 is involved in two hydrogen bonds: as a donor in an interaction with Oδ1 of Asn-14, and as an acceptor in an interaction with the NH of Lys-59. At the resolution of these structures, the distances and angles of these hydrogen bonds do not appear to differ significantly in the oxidized and reduced forms of the HiPIP. Finally, Tyr-12 and Phe-53 may fulfill the criteria defined by Hunter et al. (1991) that would allow a favorable π–π interaction to occur between them. The importance of this last interaction is difficult to evaluate due to slight differences in the solution and crystal structures of this HiPIP.

As noted above, the 2D NMR data on Y12F indicate that the overall fold of the protein is retained in this variant. Furthermore, the essentially identical chemical shifts of the Cys βCH_2 protons in reduced rcWT and Y12F indicate that the substitution of phenylalanine at position 12 does not significantly affect the geometry of the cluster ligands (Table 3). Compensatory changes in the chemical shifts of βCH_2 protons of Cys-34 and Cys-64, as well as the αCH of the latter, can be used to estimate the proportion of the two different electronic configurations that are found in oxidized HiPIP clusters (Bertini et al., 1995a). In Y12F, the βCH_2 protons of Cys-34 and the αCH Cys-64 have increased chemical shifts with respect to the corresponding signals in rcWT (Table 4). This indicates that the substitution of phenylalanine at position 12 does not affect the chemical equilibrium between the two electronic distributions within the cluster. The similarity of the temperature dependence of the chemical shifts of the hyperfine shifted signals in Y12F and rcWT supports this conclusion.

Although the quality of the 2D maps precludes an exhaustive structural analysis of Y12F, several pertinent conclusions may be drawn. Of the 11 protons whose chemical shifts differ by more than 0.15 ppm between Y12F and rcWT (Table 2 and Kinemage 1), 5 of these protons are in the immediate vicinity of the two hydrogen bonds of Tyr-12 Oη that are eliminated in the Y12F variant: 3 are on residues that hydrogen bond to Tyr-12 (Lys-59 and Asn-14), whereas the other 2 are spatially close (Ala-4 and Glu-5). Therefore, the observed variation in chemical shifts probably reflects the change in the network of hydrogen bonds involving Tyr-12. Interestingly, the signal of Lys-59 HN was not assigned in the Y12F variant. The differences in the chemical shifts of protons of Gly-46, Val-58, and Trp-45 may be explained by the fact that the NH of Gly-46 is hydrogen bonded to the carbonyl O of Val-58. A change in the hydrogen bonded state of Lys-59 NH would be transmitted directly to Val-58 O through the peptide bond connecting these residues. The different intensities of some NOEs involving Gly-46 are a further indication that the disruption of the interaction between Tyr-12 and Lys-59 influences the interaction between Gly-46 and Val-58. The change in the intensities of NOEs from Ala-60 Hα could also reflect some perturbations in this region. Finally, Trp-45 is located close to the hydrogen bond between Gly-46 and Val-58 and the peptide bond between Val-58 and Lys-59. In fact, the Trp-45 Hα is within 3 Å of the hydrogen bond between Gly-46 NH and Val-58 O. Analysis of the NOEs from Trp-45 (data not shown) shows that this residue occupies spatially equivalent positions in rcWT and Y12F, but that the packing between Trp-45 and Arg-3 is probably slightly perturbed.

Comparison of the measured ΔT_m and corresponding calculated $\Delta\Delta G_D^{app}$ for rcWT and variant HiPIPs shows these values to be monotonically related within experimental error. As shown in Table 6, substitution of Tyr-12 with phenylalanine, histidine and tryptophan results in sequential increases in both $-\Delta T_m$ and $\Delta\Delta G_D^{app}$, indicating that both values provide an appropriate measure of changes in thermal stability caused by either position-12 substitutions or pH variations.

More specifically, the DSC data indicate that the stability of rcWT *E. halophila* HiPIP-I decreases substantially between pH 10.0 and 10.8 (i.e., the T_m drops from 66.5 to 56.7 °C). This suggests that the deprotonation of one or more residues over this pH range dramatically reduces the stability of the HiPIP. Residues in the HiPIP that might titrate in this pH range include one

lysine (Lys-59) and three tyrosine residues (Tyr-12, Tyr-25, and Tyr-67). It is unlikely that one of the three arginine residues titrates in this range because the Arg side chain has a naturally high pK and, in the WT and rcWT structures, all are highly exposed to the solvent. The structures of WT and rcWT HiPIP further indicate that the side chains of Lys-59 is completely exposed to the solvent, whereas the Tyr residues are largely buried and are unlikely to titrate prior to denaturation. However, Tyr-67 is positioned such that one edge of the aromatic ring and the hydroxyl group are partially accessible to the solvent, thus the deprotonation of the hydroxyl group cannot be ruled out completely as a potential cause of the reduction in stability. The structural data show that the solvent-exposed ζ-amino group of Lys-59, whose natural pK is about 10.4, is positioned to form an ion pair with the carboxylate of Glu-61. The importance of such side-chain interactions in the stability of ferredoxins has been noted by a number of authors (Perutz & Raid, 1975; Burova et al., 1995). It is noted that disruption of a favorable ion pair between Lys-59 and Glu-61 could also be responsible for the loss in stability between pH 10 and 10.8 by changing the local electrostatic environment and by altering the conformational freedom of Lys-59, thereby weakening the critical hydrogen bond between the Lys-59 NH and Tyr-12 Oη (see below).

Packing volumes of buried Tyr and Phe residues are nearly identical, with average values of 203.6 Å^3 and 203.4 Å^3, respectively, having been reported (Chothia, 1975). The ΔT_m of −12.9 °C (see Table 6), relative to the rcWT T_m of 67.7 °C, observed for Y12F at pH 7 therefore indicates the importance of the hydrogen bonds between the Tyr-12 hydroxyl and Asn-14 and the backbone of Lys-59 to the structural stability of *E. halophila* HiPIP-I (Kinemage 1). Hydrogen bonds between uncharged donors and acceptors have been estimated to contribute 0.5–1.5 kcal/mol to protein stability (Dill, 1990). The $\Delta\Delta G_D^{app}$ of Y12F at pH 7.0 of 2.3 kcal/mol is therefore consistent with the loss of two hydrogen bonds contributing to the stability of the HiPIP. The relative stability of the Y12F variant, in terms of either ΔT_m or $\Delta\Delta G_D^{app}$, is approximately constant between pH 7 and 10, but jumps dramatically when the pH is increased to 10.8. This further suggests that deprotonation of Lys-59 is at least partially responsible for the dramatic reduction in the stability of both rcWT and Y12F between pH 10 and 10.8.

Destabilization energies in excess of those for Y12F are observed for position-12 variants which, in addition to eliminating favorable hydrogen bonds, alter the local packing density and hydrophobicity. Among the purified variants, introduction of tryptophan at position 12 leads to the largest loss in stability, presumably because of the significant perturbations in the local structure needed to accommodate the larger Trp side-chain (237.6 Å^3 internal packing volume). The relative hydrophobicity (0.5 kcal/mol) and the average packing volume (167.3 Å^3) are significantly smaller for His than for Tyr (2.3 kcal/mol, 203.6 Å^3). Both of these factors are therefore likely to contribute to the observed decrease in Y12H stability relative to that of Y12F at pH 7. The steps required to express Y12I and Y12A and the subsequent attempts to purify them indicate that these variants are less stable than Y12W. Although isoleucine and alanine have smaller packing volumes than tyrosine (168.8 Å^3 and 91.5 Å^3, respectively) and lack the hydrogen bonding capabilities of the latter, the extreme instability of the Y12I and Y12A variants suggests that electrostatic interactions between Tyr-12 and either the cluster or Phe-53 (aromatic–aromatic interaction, see above) further stabilize the HiPIP. Although the ring of Tyr-12 flips, aromatic–aromatic interactions have previously been shown not to be hindered by ring flipping (Serrano et al., 1991).

Carter (1977) correlated the presence of Tyr-12 with the bands of negative ellipticity in the CD spectrum of reduced *C. vinosum* HiPIP at 348 and 394 nm. It was further predicted that disruption of the hydrogen bond network involving Tyr-12 Oη would decrease the rotational strength of the cluster by destabilizing the charge–dipole interaction between the cluster and the tyrosine. A subsequent study of 13 HiPIPs showed that no correlation between the tyrosine and the negative CD bands exists, partly because the CD spectrum of reduced *E. halophila* HiPIP-I shows positive bands in this region (Przysiecki et al., 1985). In the present study, the similarity of the CD spectra of rcWT and Y12F clearly demonstrate that loss of the hydrogen bonding to the tyrosine does not influence the rotational strength of the cluster. The CD spectra of the Y12H and Y12W variants demonstrate that Tyr-12 perturbs several electronic transitions in the cluster, including those occurring in the region identified by Carter, although it cannot be ruled out that the observed spectral perturbations are due to structurally induced changes in other aromatic residues, such as Phe-53 and Trp-45. Hsu and Woody (1971) concluded that in hemeproteins, π–π^* transitions of aromatic residues, especially tyrosine and tryptophan residues, up to 15 Å from the prosthetic group can influence the electronic transitions of the heme through a coupled oscillator interaction. By analogy, it is reasonable to expect that most of the 11 aromatic residues in *E. halophila* HiPIP-I could perturb cluster transitions by a similar coupled oscillator mechanism. Finally, it is noted that the flipping of the Tyr-12 ring indicates that ring flipping does not hinder coupled oscillator interactions. Indeed, the fast flipping Phe-82 in yeast iso-1-cytochrome *c* is the principle determinant of the intense negative Cotton effect in the Soret CD spectrum of the oxidized cytochrome (Pielak et al., 1986; Rafferty et al., 1990).

The charge–dipole interaction between the HiPIP cluster and Tyr-12 has been suggested to be stronger in the reduced state of the protein (Carter, 1977), and should therefore influence the latter's reduction potential. Elimination of the Tyr-12 hydroxyl group, in weakening the interaction, should thus lower the reduction potential of the HiPIP. Because the reduction potential of Y12F is higher than that of rcWT (Table 7), the position-12 substitutions apparently influence the reduction potential of the cluster in another manner. For example, the current stability and structural data indicate that the close packing of the molecule around position 12 is disrupted in the variants. Armstrong et al. (1990) have ascribed the negative entropy associated with the reduction of *C. vinosum* HiPIP to an increase in the solvent ordering or a more compact conformation of the reduced protein. The less negative entropies of reduction of the position-12 *E. halophila* HiPIP variants versus rcWT could arise because the increase in compactness upon reduction of the variants is not as great as in rcWT. The introduction of Fl-Tyr at this position of the *C. vinosum* HiPIP raises the reduction potential of this HiPIP by 30 mV and has been cited as evidence for electronic coupling between this residue and the cluster (Lui & Cowan, 1994). This substitution is undoubtedly less disruptive than any of the substitutions at position 12 of the *E. halophila* HiPIP studied here.

The variation in the reduction potential of the position-12 HiPIP variants is not great and could easily be acheived by changes in other residues that would not otherwise alter the function of the protein. Furthermore, electron transfer in HiPIPs has been proposed to occur through the surface of the protein involving Phe-36 (Bertini et al., 1993) and would presumably not involve Tyr-12. The orientation of Tyr-12 appears to be conserved in other HiPIPs, as is the nearby Phe-53 in many of these proteins. Taken together with the current results, we conclude that the principle selective pressure on maintaining tyrosine at position 12 of *E. halophila* HiPIP-I is the stabilization of the protein, both through hydrogen bonds involving the tyrosyl hydroxyl group, and favorable electrostatic interactions between the aromatic ring and the cluster and/or a nearby aromatic residue.

Materials and methods

Bacterial strains and plasmids

Variant HiPIPs were created and expressed using pLEHP20, a derivative of pEMBL18 containing a synthetic gene encoding *E. halophila* HiPIP iso-I as a fusion protein (Eltis et al., 1994). *Escherichia coli* XL-1 Blue (Stratagene, La Jolla, California) was used for routine propagation of plasmid DNA. Expression of protein from pEMBL18 constructs was done in *E. coli* strains XL-1 Blue and LE392. The expression of Y12A and Y12I from pT7-7 derivatives (Tabor & Richardson, 1985) was investigated in *E. coli* BL21(DE3) (Studier & Moffatt, 1986). *E. coli* strains CJ236 and RZ1032 and helper phage R408 were used in the preparation of uracil-containing ssDNA. Strains used for protein expression were grown in superbroth containing 200 mg/L of ampicillin, 50 mg/L of tetracycline, and 50 mg/L of chloramphenicol, as appropriate. For all other purposes, LB broth supplemented with appropriate antibiotics was used.

Manipulation of DNA

DNA was manipulated using standard protocols (Ausubel et al., 1991). Oligonucleotide-directed mutagenesis was performed essentially as described by Smith (1986) using a uracil-containing single-stranded template (Kunkel, 1985). Oligonucleotides were synthesized on an Applied Biosystems, Inc. (ABI) model 38013 DNA synthesizer and were extracted with butanol prior to use (Sawadogo & Van Dyke, 1991). The oligonucleotides used to generate the position-12 variants, together with the resulting plasmids, are listed in Table 1. All strains were transformed by electroporation using a Bio-Rad Gene Pulser (Hercules, CA) transfection apparatus and pulse controller according to the manufacturer's recommendations, except *E. coli* BL21(DE3), which was transformed using the calcium chloride method. Plasmid DNA was sequenced using an ABI model 373 DNA sequencer interfaced to a Macintosh IIcx microcomputer. Plasmid DNA was purified for sequencing on QIAwell-8 columns (QIAGEN, Inc., Chatworth, California) according to the instructions of the manufacturer. Sequencing reactions were performed according to the ABI dye-deoxy terminator protocol using either HiPIP8 (5'-GGCGACTAGTCATCACCATC-3'), M13 universal, or M13 reverse primers.

Expression and protein purification

The expression of variant HiPIPs was evaluated in cultures of 50 or 150 mL. The cells were harvested and either frozen at −20 °C before use or immediately suspended in 5 mL of lysis buffer (20 mM phosphate, pH 8.0). Cellular extracts were prepared using a French Pressure cell as described previously (Eltis et al., 1994). Recombinant protein was extracted from the supernatant of cellular extracts using a 75-μL slurry of Invitrogen Pro-Bond resin in an eppendorf tube. After washing the resin two times with 1 mL of lysis buffer and wash buffer (20 mM phosphate, 300 mM sodium chloride, 10% glycerol, pH 6.0), the recombinant proteins was eluted from the resin with 150 μL of 200 mM imidazole. Five microliters of this eluate was analyzed by SDS-PAGE.

For biophysical characterization, protein was purified from cultures of 5–20 L. Variant HiPIPs were purified by nickel resin and anion exchange chromatography essentially in the same manner as recombinant wild-type HiPIP iso-I (rcWT; Eltis et al., 1994). A final gel filtration step was introduced by concentrating the appropriate fractions obtained from the anion exchange step to a volume of 5 mL. This was loaded onto a Superdex G75 HR 26/60 gel filtration column (Pharmacia Biotech Inc., Québec) and eluted at 2 mL/min in 20 mM MOPS, 200 mM sodium chloride, pH 7.0. Fractions containing HiPIP were pooled, concentrated, and frozen in liquid nitrogen for future use.

The semi-anaerobic purification of some variants was achieved by continually flushing all chromatography buffers with argon during their use and supplementing them with 1 mM dithiothreitol. Cells were lysed in the usual method. The resulting extract was centrifuged twice at 15,000 rpm and filtered through a 0.45-μM filter before being loaded onto a MonoQ HR10/10 column as described for the other proteins. The eluted protein was collected in an argon-flushed Amicon stirred-cell concentrator, concentrated, and exchanged into cleavage buffer under nitrogen at 4 °C. The polyhistidine leader sequence was removed with Factor Xa at room temperature for 1 h under argon. The cleaved protein was further purified on a Superdex G75 26/60 column equilibrated with argon-flushed buffers containing 1 mM dithiothreitol as described above. The HiPIP was again collected and concentrated in an argon-flushed stirred-cell. Semi-anaerobically purified HiPIPs were stored at −70 °C and thawed under a stream of humidified argon as required.

Manipulation of protein and electrophoresis

HiPIP concentrations were determined spectrophotometrically by using the difference in the extinction coefficients of the oxidized and reduced forms of the protein at 500 nm, $\Delta\epsilon_{500}$ = 8.6 mM^{-1} cm^{-1} (Przysiecki et al., 1985). Both the purity and the cluster content of the HiPIP were monitored by measuring the *R*-value (A_{280}/A_{379}) of the oxidized protein. Protein samples were concentrated and exchanged into appropriate buffers using dialysis tubing and Amicon (Beverly, Massachusetts) Centricons, Centripreps, and stirred-cell concentrators. Oxidized HiPIP was prepared by adding a small excess of ammonium bis(dipicioloinato)cobalt(III) (Mauk et al., 1979), which was subsequently removed by passage of the sample over a short gel filtration column equilibrated with the appropriate buffer. HiPIP was reduced with the addition with a few grains of sodium dithionite. SDS-polyacrylamide gels containing 15–17%

acrylamide were electrophoresed on a Bio-Rad Miniprotean II apparatus according to standard procedures (Ausubel et al., 1991). Protein bands were visualized using Coomassie Blue. Low molecular protein weight markers from Bio-Rad were used.

^{1}H NMR spectroscopy

All NMR experiments were recorded on a Bruker AMX 600 spectrometer. One-dimensional experiments were recorded over spectral windows of 20 kHz and 125 kHz for reduced and oxidized forms, respectively. The spectra were calibrated by assigning a chemical shift of 4.81 ppm from DSS to the H_2O signal at 298 K. Selective irradiation with a weak RF field was used to reduce the strong solvent signal.

NOESY experiments (Macura et al., 1982) were collected on the reduced Y12F derivative using the same parameters as experiments performed on rcWT (Bertini et al., 1994b); 4,096 × 973 data points were acquired, 96 scans each, using mixing and recycle delays of 100 ms and 1,100 ms, respectively. Data were acquired in the TPPI mode (Marion & Wüthrich, 1983). Squared cosine bell weighting functions were used to multiply experimental data prior to zero filling and Fourier transformation in both dimensions. The final size of the data set was 2,048 × 1,024 points.

CD

CD measurements were performed on a JASCO J-720 spectropolarimeter equipped with a Neslab (Newinton, New Hampshire) RTE-110 circulating waterbath. The CD instrument was interfaced to an ANO 386 microcomputer. Immediately prior to use, the instrument was calibrated with a 0.06% ammonium *d*-10 camphorsulfonic acid according to the procedure provided with the instrument. Spectra were collected between 300.0 and 700.0 nm with a band width of 1 nm and a sensitivity of 50 mdeg. Samples of approximately 40 μM of protein were initially oxidized and exchanged into 80 M HEPES, 0.1 M sodium chloride, pH 7.0. Three scans were averaged to obtain each final spectrum. Recorded values were converted to molar ellipticities.

DSC

DSC experiments were carried out using a Hart model 4215 DSC set at a temperature scan rate of 1 °C/min. Protein concentrations ranged from 1.5 to 2.7 mg/mL and each calorimetry cell contained 0.5 mL of sample referenced against a near equal (heat-capacity matched) volume of reference buffer. At each pH, two to eight independent sample preparations of rcWT or variant protein were run to establish data reproducibility and errors. Each protein thermogram was background corrected for the thermogram of the buffer solution. The buffers used included 20 mM MOPS, pH 7.0; 20 mM TAPS, pH 9.0; 20 mM CAPS, pH 10.0; 20 mM CHES, pH 10.8; and 40 mM piperidine, pH 11.0.

Electrochemistry

The midpoint reduction potentials of rcWT and variant HiPIPs were determined by cyclic voltammetry using a Princeton Applied Research model 273A potentiostat/galvanostat. A freshly polished pyrolitic graphite disc (edge plane) served as the working electrode. A platinum sheet and the standard calomel electrode were used as the counter and reference electrodes, respectively. Protein samples were exchanged into 20 mM MOPS, 0.2 M NaCl, pH 6.98, containing 2 mM neomycin as a promotor. Prior to each experiment, the working electrode was polished with alumina (BDH, particle size 0.075 μm) and cleaned with distilled water in an ultrasonication bath. The pH of the protein sample was determined immediately before and after each electrochemical measurement. Variation of the scan rate between 0.01 and 0.1 V/s did not influence the measured reduction potential. The midpoint reduction potential of the Y12F variant in 20 mM HEPES, 80 mM sodium chloride, pH 7.0 was also measured using an optically transparent thin-layer electrode cell following the same procedure as that used to determine that of the rcWT HiPIP (Eltis et al., 1994).

Acknowledgments

We thank Dr. John Hobbs, Tracy Farr, Tracy Evans, and Debra Neufeld of the NAPS unit of the Biotechnology Laboratory at UBC for the synthesis of oligonucleotides and running the sequencing gels. We also thank Gary Lesnecki for his assistance in the large-scale growth of cultures, and Dr. A. Grant Mauk for the use of the CD spectropolarimeter, which was purchased with funds from the Protein Engineering Network for Centres of Excellence. The enthusiasm and support of Drs. Ivano Bertini, Claudio Luchinat and Michael Smith, in whose respective laboratories some of this research was performed, are greatly appreciated.

References

Antanaitis BC, Moss TH. 1975. Magnetic studies of the four-iron high-potential, non-heme protein from *Chromatium vinosum*. *Biochim Biophys Acta 405*:262–279.

Agarwal A, Tan J, Eren M, Tevelev A, Lui SM, Cowan J. 1993. Synthesis, cloning and expression of a synthetic gene for high potential iron protein from *Chromatium vinosum*. *Biochem Biophys Res Comm 197*:1357–1362.

Armstrong FA, Butt JN, Govindaraju K, McGinnis J, Powls, Sykes AG. 1990. Direct cyclic voltammetry of three ruthenium-modified electron-transfer proteins. *J Inorg Chem 29*:4858–4862.

Ausubel FM, Brent R, Kingston RE, Moore DD, Seidman JG, Smith JA, Struhl K. 1991. *Current protocols in molecular biology*. New York: Greene Publishing Associates.

Babini E, Bertini I, Borsari M, Capozzi F, Dikiy A, Eltis LD, Luchinat C. 1995. A serine to cysteine ligand mutation in the high potential iron sulfur protein from *Chromatium vinosum* provides insight into the electronic structure of the 4Fe-4S cluster. *J Am Chem Soc*. In press.

Backes G, Mino Y, Loehr TM, Meyer TE, Cusanovich MA, Sweeney WV, Adman ET, Sanders-Loehr J. 1991. The environment of Fe4S4 clusters in ferredoxins and high-potential iron proteins. New information from X-ray crystallography and resonance Raman spectroscopy. *J Am Chem Soc 113*:2055–2064.

Banci L, Bertini I, Ciurli S, Luchinat C, Pierattelli R. 1995a. Rationalization of the reduction potentials within the series of the high-potential iron-sulfur proteins. *Inorg Chim Acta*. Forthcoming.

Banci L, Bertini I, Dikiy A, Kastrau DHW, Luchinat C, Sonpornpisut P. 1995b. The tridimensional solution structure of the reduced high potential iron sulfur protein from *Chromatium vinosum* through NMR. *Biochemistry 34*:206–219.

Banci L, Bertini I, Eltis LD, Felli IC, Kastrau DHW, Luchinat C, Piccioli M, Pierattelli R, Smith M. 1994. The three-dimensional structure in solution of the paramagnetic high-potential iron-sulfur protein I from *Ectothiorhodospira halophila* through nuclear magnetic resonance. *Eur J Biochem 225*:715–725.

Bartsch RG. 1978. High potential iron proteins: Bacterial. *Methods Enzymol 53*:329–340.

Becktel WJ, Schellman JA. 1987. Protein stability curves. *Biopolymers 26*: 1859–1877.

Beinert H, Kennedy MC. 1989. Engineering of protein bound iron-sulfur clusters. *Eur J Biochem 186*:5–15.

Benning MM, Meyer TE, Rayment I, Holden HM. 1994. Molecular structure of the oxidized high potential iron-sulfur protein isolated from *Ectothiorhodospira vacuolata*. *Biochemistry 33*:2476–2483.

Bertini I, Briganti F, Luchinat C, Scozzafava A, Sola M. 1991. ^{1}H NMR

spectroscopy and the electronic structure of the high potential iron-sulfur protein from *Chromatium vinosum*. *J Am Chem Soc 113*:1237-1245.

Bertini I, Capozzi F, Eltis LD, Felli IC, Luchinat C, Piccioli M. 1995a. Sequence-specific assignment of oxidized, recombinant HiPIP I from *Ectothiorhodospira halophila*. *Inorgan Chem 34*:2516-2523.

Bertini I, Capozzi F, Luchinat C, Piccioli M, Vila AJ. 1994a. The Fe_4S_4 centers in ferredoxins studied through proton and carbon hyperfine coupling. Sequence specific assignments of cysteines in ferredoxins from *Clostridium acidi urici* and *Clostridium pasteurianum*. *J Am Chem Soc 116*:651-660.

Bertini I, Eltis LD, Felli IC, Luchinat C, Piccioli M. 1995b. Solution structure of oxidized, recombinant HiPIP I from *Ectothiorhodospira halophila*. *Chemistry*. Forthcoming.

Bertini I, Felli IC, Kastrau DHW, Luchinat C, Piccioli M, Viezzoli MS. 1994b. Sequence-specific assignment of the ^1H and ^{15}N nuclear magnetic resonance spectra of the reduced recombinant high-potential iron-sulfur protein I from *Ectothiorhodospira halophila*. *Eur J Biochem 225*: 703-714.

Bertini I, Gaudemer A, Luchinat C, Piccioli M. 1993. Electron self-exchange in high-potential iron-sulfur proteins. Characterization of protein I from *Ectothiorhodospira vacuolata*. *Biochemistry 32*:12887-12893.

Betz SF, Pielak GJ. 1992. Introduction of a disulfide into cytochrome *c* stabilizes a compact denatured state. *Biochemistry 31*:12337-12344.

Breiter DB, Meyer TE, Rayment I, Holden HM. 1991. The molecular structure of the high potential iron-sulfur protein isolated from *Ectothiorhodospira halophila* determined at 2.5 Å resolution *J Biol Chem 266*: 18660-18667.

Burova TV, Bernhardt R, Pfeil W. 1995. Conformational stability of bovine holo and apo adrenodoxin – A scanning calorimetry study. *Protein Sci 4*: 909-916.

Cammack R. 1973. Super reduction of chromatium high potential iron-sulfur protein in the presence of dimethyl sulfoxide. *Biochem Biophys Res Commun 54*:548-554.

Carter CW Jr. 1977. New stereochemical analogies between iron-sulfur electron transport proteins. *J Biol Chem 252*:7802-7811.

Carter CW Jr, Kraut J, Freer ST, Alden RA, Sieker LC, Adman E, Jensen LH. 1972. A comparison of Fe_4S_4 clusters in high potential iron protein and in ferredoxin. *Proc Natl Acad Sci USA 69*:3526-3529.

Carter CW Jr, Kraut J, Freer ST, Xuang NH, Alden RA, Bartsch RG. 1974b. Two-Ångstrom crystal structure of oxidized *Chromatium* high potential iron protein. *J Biol Chem 249*:4212-4225.

Chothia C. 1975. Structural invariants in protein folding. *Nature 254*:304-308.

Eltis LD, Iwagami SG, Smith M. 1994. Hyperexpression of a synthetic gene encoding a high potential iron sulfur protein. *Protein Eng 7*:1145-1150.

Freire E, Biltonen RL. 1978. Statistical mechanical deconvolution of thermal transitions in macromolecules: I. Theory and application to homogeneous systems. *Biopolymers 17*:463-479.

Freire E, van Osdol WW, Mayorga OL, Sanchez-Ruiz JM. 1990. Calorimetrically determined dynamics of complex folding transitions in proteins. *Annu Rev Biophys Biophys Chem 19*:159-188.

Hsu MC, Woody RW. 1971. The origin of the heme Cotton effects in myoglobin and hemoglobin. *J Am Chem Soc 93*:3515-3525.

Hunter CA, Singh J, Thornton JM. 1991. π-π Interactions: The geometry and energetics of phenylalanine-phenylalanine interactions in proteins. *J Mol Biol 218*:837-846.

Jensen GM, Warshel A, Stephens PJ. 1994. Calculation of the redox potentials of iron-sulfur proteins: The 2-/3-couple of $[Fe_4S_4Cys_4]$ clusters in *Peptococcus aerogenes* ferredoxin, *Azotobacter vinelandii* ferredoxin I, and *Chromatium vinosum* high-potential iron protein. *Biochemistry 33*:10911-10924.

Khoroshilova N, Beinert H, Kiley PJ. 1995. Association of a polynuclear iron-sulfur center with a mutant FNR protein enhances DNA binding. *Proc Natl Acad Sci USA 92*:2499-2503.

Kim J, Rees DC. 1992. Structural models for the metal centers in the nitrogenase molybdenum-iron protein. *Science 257*:1677-1682.

Kunkel TA. 1985. Rapid and efficient site-specific mutagenesis without phenotypic selection. *Proc Natl Acad Sci USA 82*:488-492.

Lui SM, Cowan JA. 1994. Studies of the electronic and dynamic properties of high potential iron proteins by substitution with non-natural amino acids. 3-Fluorotyrosine-modified *Chromatium vinosum* high-potential iron protein. *J Am Chem Soc 116*:4483-4484.

Macura S, Wütrich K, Ernst RR. 1982. The relevance of J cross-peaks in two-dimensional NOE experiments of macromolecules. *J Magn Reson 47*:351-357.

Marion D, Wüthrich K. 1983. Application of phase sensitive correlated spectroscopy (COSY) for measurements of proton-proton spin-spin coupling constant in proteins. *Biochem Biophys Res Commun 113*:967-974

Matouschek A, Matthews JM, Johnson CM, Fersht AR. 1994. Extrapolation to water of kinetic and equilibrium data for the unfolding of barnase in urea solutions. *Protein Eng 7*:1089-1095.

Mauk AG, Coyle CL, Brodignon E, Gray HB. 1979. Bis(dipicolinate) complexes of cobalt(III) and iron (II) as new probes of electron-transfer reactivity. Analysis of reactions involving cytochrome *c* and cytochrome c_{551}. *J Am Chem Soc 101*:5054-5056.

Middleton P, Dickson DPE, Johnson CE, Rush JD. 1980. Interpretation of the Mössbauer spectra of the high-potential iron protein from *Chromatium*. *Eur J Biochem 104*:289-296.

Orme-Johnson NR, Mims WB, Orme-Johnson WH, Bartsch RG, Cusanovich MA, Peisach J. 1983. Oxidation state dependence of proton exchange near the iron-sulfur centers in ferredoxin and high-potential iron-sulfur proteins. *Biochim Biophys Acta 748*:68-72.

Perutz MF, Raid H. 1975. Stereochemical basis of the heat stability in bacterial ferredoxin and in haemoglobin A2. *Nature 255*:256-259.

Pielak GJ, Oikawa K, Mauk AG, Smith M, Kay CM. 1986. Elimination of the negative Soret Cotton effect of cytochrome *c* by replacement of the invariant phenylalanine using site-directed mutagenesis. *J Am Chem Soc 108*:2724-2727.

Privalov PL, Potekhin SA. 1986. Scanning microcalorimetry in studying temperature-induced changes in proteins. *Methods Enzymol 131*:4-51.

Przysiecki CT, Meyer TE, Cusanovich MA. 1985. Circular dichroism and redox properties of high redox potential ferredoxins, *Biochemistry 24*: 2542-2549.

Rafferty SP, Pearce LL, Barker PD, Guillemette JG, Kay CM, Smith M, Mauk AG. 1990. Electrochemical, kinetic, and circular dichroic consequences of mutations at position 82 of yeast iso-1-cytochrome *c*. *Biochemistry 29*:9365-9369.

Rayment I, Wesenberg G, Meyer TE, Cusanovich MA, Holden HM. 1992. Three-dimensional structure of the high potential iron-sulfur protein isolated from the purple phototrophic bacterium *Rhodocyclus tenuis* determined and refined at 1.5 Å resolution. *J Mol Biol 228*:672-686.

Sawadogo M, Van Dyke MW. 1991. A rapid method for the purification of deprotected oligodeoxynucleotides. *Nucleic Acid Res 19*:674.

Serrano L, Bycroft M, Fersht AR. 1991. Aromatic-aromatic interactions and protein stability investigations by double-mutant cycles. *J Mol Biol 218*: 465-475.

Sheridan RP, Allen LC, Carter CW Jr. 1981. Coupling between oxidation state and hydrogen bond conformation in high potential iron-sulfur protein. *J Biol Chem 256*:5052-5057.

Smith M. 1986. In vitro mutagenesis. *Annu Rev Genet 19*:423-463.

Studier FW, Moffatt BA. 1986. Use of bacteriophage T7 RNA polymerase to direct selective expression of cloned genes *J Mol Biol 189*:113-130.

Tabor S, Richardson CC. 1985. A bacteriophage T7 RNA polymerase/promotor system for controlled exclusive expression of specific genes. *Proc Natl Acad Sci USA 82*:1074-1078.

Volbeda A, Charon MH, Piras C, Hatchikian EC, Frey M, Fontecilla-Camps JC. 1995. Crystal structure of the nickel-iron hydrogenase from *Desulfovibrio gigas*. *Nature 373*:580-586.